Microscopic Observation of Pauli Blocking in Degenerate Fermionic Lattice Gases

Ahmed Omran,[1,*] Martin Boll,[1] Timon A. Hilker,[1] Katharina Kleinlein,[1] Guillaume Salomon,[1] Immanuel Bloch,[1,2] and Christian Gross[1]

[1]*Max-Planck-Institut für Quantenoptik, 85748 Garching, Germany*

[2]*Ludwig-Maximilians-Universität, Fakultät für Physik, 80799 München, Germany*

(Received 15 October 2015; published 23 December 2015)

The Pauli exclusion principle is one of the most fundamental manifestations of quantum statistics. Here, we report on its local observation in a spin-polarized degenerate gas of fermions in an optical lattice. We probe the gas with single-site resolution using a new generation quantum gas microscope avoiding the common problem of light induced losses. In the band insulating regime, we measure a strong local suppression of particle number fluctuations and a low local entropy per atom. Our work opens a new avenue for studying quantum correlations in fermionic quantum matter both in and out of equilibrium.

DOI: 10.1103/PhysRevLett.115.263001 PACS numbers: 67.85.Lm, 07.60.Pb, 37.10.De

Quantum statistics distinguishes between two fundamentally different kinds of particles: bosons, which condense into a single quantum state at zero temperature, and fermions, for which multiple occupancy of a single state is forbidden. As a result, identical fermions seem to repel each other, described by an effective Fermi pressure on a macroscopic level [1]. Microscopically, the Pauli blockade manifests itself in a strong suppression of density fluctuations [2,3] and in antibunching of density-density correlations [4–9]. Specifically, fermions in periodic potentials form a band insulating state with suppressed number fluctuations on each site when the chemical potential lies in the band gap. Measuring these number fluctuations can therefore be regarded as a direct probe of Pauli blocking.

Local fluctuations in periodic potentials have been directly studied with ultracold bosonic atoms in optical lattices [10–12]. Some of these experiments featured site-resolved fluorescence detection with single atom sensitivity [13,14], which has proven to be a powerful method for probing quantum many-body systems. However, such quantum gas microscopy requires a specialized experimental setup with considerably increased technical complexity. In particular, the often used fermionic alkali atoms are difficult to laser cool, making the single-site and atom resolved detection even more challenging. First results have recently been reported on the imaging of single fermions in dilute thermal clouds [15–18]. However, microscopy of quantum degenerate fermions has so far remained out of reach.

Here, we report on the site-resolved characterization of a spin-polarized degenerate Fermi gas in an optical lattice. In the band-insulating region, we measure a strong suppression of local atom number fluctuations, more than one order of magnitude below the Poisson limit expected for uncorrelated particles. Based on the measurement of the local occupation statistics, we reconstruct the spatial entropy distribution in the inhomogeneous samples. We obtained these results with a conceptionally novel quantum gas microscope based on an additional, dedicated optical lattice for detection. This provides high flexibility for future experiments and offers an alternative approach [19,20] to overcome the limitations due to parity detection [12,14].

Our experiments started in a standard magneto-optical trap of ^{6}Li loaded from a Zeeman slower [21]. We further cooled the atoms using narrow-line laser cooling on the 323 nm line [23,24]. The resulting 50/50 spin mixture of fermions in the $|F, m_F\rangle = |1/2, \pm 1/2\rangle$ states was then loaded into an optical trap and evaporatively cooled at a magnetic field controlled scattering length of $a_{\mathrm{evap}} = -290 a_B$, where a_B is the Bohr radius. Next, we transported the atoms into a glass cell, where we used a further, vertically propagating optical dipole trap to locally enhance the density for a second efficient optical evaporation at a_{evap}. To reduce the vertical extension of the cloud, the atoms were transferred into a strongly elliptical dimple trap with a vertical waist of $w_z = 1.7$ μm. Two beams were shone in from the side, which interfered under a small angle to produce a vertical optical lattice of 3 μm spacing as illustrated in Fig. 1(a). The fermions loaded from the dimple trap populated mostly a single plane of this optical lattice. However, for high fidelity microscopy, almost all atoms in the adjacent planes need to be removed. This was achieved by transferring the atoms in undesired planes in a vertical magnetic field gradient from the $|1/2, \pm 1/2\rangle$ to the $|3/2, \mp 1/2\rangle$ states, which are subsequently lost due to spin changing collisions. The atoms in the final single plane were evaporatively cooled at a_{evap}, using a horizontal magnetic field gradient. The radial confinement counteracting this gradient was set independently by the depth of the vertical dipole trap. To produce a spin-polarized sample, we ramped the magnetic field to 27 G, where the magnetic moment of only the $|1/2, -1/2\rangle$ spin state vanishes. Then, we reduced the in-plane confinement until the gradient field completely removed the $|1/2, +1/2\rangle$ spin component, which we verified using Stern-Gerlach separation.

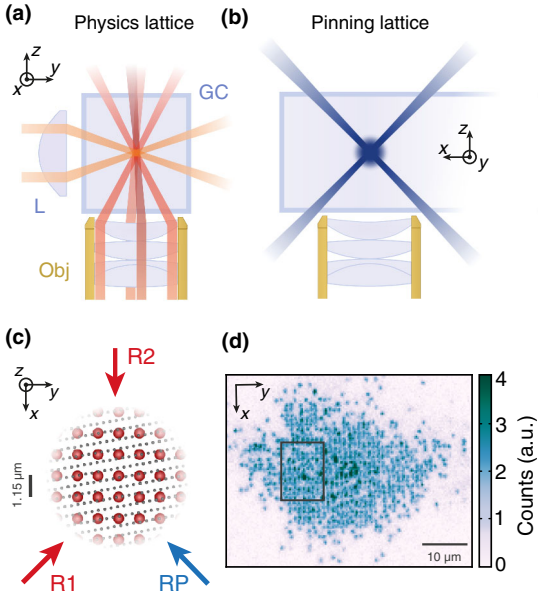

FIG. 1 (color online). Experimental setup. (a) Geometry of the physics lattice. A vertical standing wave of 3 μm spacing is produced by focusing two beams with an aspheric lens (L) onto the atoms from the side. The horizontal lattice with a spacing of 1.15 μm is formed by two pairs of beams focused through the imaging objective (Obj) beneath the glass cell (GC). (b) Pinning lattice beams viewed from the side. Two beams propagate close to the imaging objective in the x-z plane, while the third beam is in the y direction. All beams are retroreflected, forming a 532 nm lattice. (c) Pinning lattice oversampling and Raman beam geometry viewed from top. For imaging, the atoms are loaded from the physics lattice (red dots) to the pinning lattice (gray dots). The Raman beams (red, R1 and R2) and repump beam (blue, RP) propagate in the x-y plane. For the pinning lattice, we show the sites within ± 250 nm from one x-y plane of the physics lattice. In the experiment the relative position between pinning and physics lattice sites is not controlled. (d) Fluorescence image of $N = 763(10)$ ^{6}Li atoms acquired over 1 s of Raman sideband cooling. The black box marks the region where we evaluated the fluorescence statistics shown in Fig. 2.

The optical lattice was tailored to the properties of ^{6}Li, especially to its light mass m. In a lattice, the single particle energy scale is given by the recoil energy $E_R = h^2/8ma_l^2$, such that the lattice constant a_l can be large when the mass is small. For lithium, fast tunneling time scales in the kilohertz regime are realized even for $a_l > 1$ μm. Thus, the strongly correlated regime is experimentally accessible, given the availability of Feshbach resonances to tune the interactions [25]. We loaded the atoms into such a large scale two-dimensional "physics" lattice with $a_l = 1.15\,\mu$m, produced by focusing phase coherent pairs of parallel beams with a custom microscope objective (numerical aperture 0.5, effective focal length 28 mm). The same objective was later used to collect the fluorescence signals during imaging [see Fig. 1(a)].

We used a deep additional "pinning" lattice with a lattice spacing of 532 nm that oversampled the physics lattice [see Figs. 1(b),1(c)] [26]. The 1064 nm pinning lattice beams were retroreflected with waists of 56 μm and an average power of 22 W per direction, resulting in an overall trap depth of 2.5 mK and on-site trap frequencies of 1.3 MHz on all axes. Prior to imaging, we transferred the atoms to the pinning lattice, which provides sufficient local confinement for Raman sideband cooling [27–29] with a Lamb-Dicke parameter $\eta \approx 0.23$. The Raman cooling [21] was optimized for high fidelity imaging. The scattered photons provided the fluorescence signal [see Fig. 1(d)], which we detected with an electron-multiplied CCD camera [30,31]. Over a detection period of 1 s, we collected on average 350 photons per atom, corresponding to a fluorescence rate of about 7 kHz. Parasitic background light was negligible during the 1 s exposure.

We reconstruct the physics lattice population via a local image analysis based on the point-spread function (PSF) of the detection system. We extract the PSF from fluorescence images of sparsely filled atomic samples by averaging many isolated single atom signals. This experimentally determined PSF is well approximated by a Gaussian with a standard deviation of 380(10) nm, considerably larger than the specified and independently confirmed 290 nm. The first step of the reconstruction algorithm is to identify the position of the physics lattice on each single image by Fourier transforming the image and extracting the phase associated with the lattice wave vectors. The resulting physics lattice grid is shown in the inset of Fig. 2. Even though the atoms were held in the incommensurate pinning lattice during imaging, a clear distinction of empty and singly occupied physics lattice sites is visible on the bare

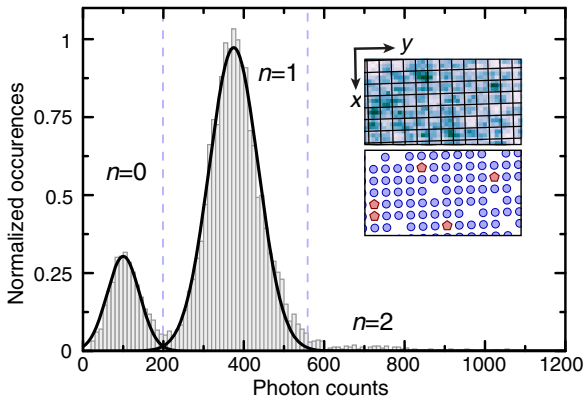

FIG. 2 (color online). Lattice reconstruction. Statistics of fluorescence levels obtained from the amplitude of local Gaussian fits per site. On 50 images, we evaluated the region marked in black in Fig. 1(d) with an average filling of 85%. The peaks in the histogram of $n = 0$ and $n = 1$ atoms are clearly separated (black lines are Gaussian fits). The few counts to the right are due to double occupancies [21]. The dashed lines mark the thresholds for identifying zero, one, and two atoms per site. Inset: Close-up of an exemplary fluorescence image with the results of the reconstruction shown below. Single atoms are marked with blue dots, red pentagons indicate double occupancies.

fluorescence image. Next, we determine the photon counts in each physics lattice site from a fit with the Gaussian approximated PSF. The resulting histogram of the fit amplitudes for images around unity filling [cf. Fig. 1(d)] per site is shown in Fig. 2. The peaks corresponding to empty and singly occupied sites are clearly distinct, resulting in a high fidelity of 99% for discriminating them. Furthermore, the histogram shows several events of high counts to the right of the $n = 1$ peak. We attribute these to doubly occupied physics lattice sites, which we identify with a reduced fidelity of $\simeq$70% [21]. We expect to improve on the latter in future experiments, as the detection fidelity for double occupancies is at present mainly limited by our broadened PSF.

To estimate the influence of loss and hopping events, we took subsequent images of the same sparsely populated sample with 1 s exposure per image. We found a loss probability of 2.5(5)% and a tunneling probability of 5(1)% between two images averaged over a large detection region of 50×50 μm, where most of these events occur towards the edge of this region.

Next, we used the microscope to study the local statistics of spin-polarized, degenerate fermionic samples. After evaporation and spin polarization, we ramped up the physics lattice adiabatically within 100 ms to $8E_R$. Before imaging, we rapidly increased the physics lattice depth to $20E_R$ to freeze the atomic distribution. Then we switched on the pinning lattice linearly within 5 ms. Setting the atom number between $N = 700$ and $N = 800$ fermions, we obtained images with high filling factors in the center of the trap [cf. Fig. 1(d)]. We took 425 images following this protocol and analyzed the local statistics of population for each lattice site. In the analysis, we took systematic errors due to the reconstruction as well as statistical uncertainties into account [21].

The fermionic character of the gas is directly visible in the mean density $\langle \hat{n}_i \rangle$ per site i, shown in Fig. 3(a). In an inhomogeneously trapped sample, Pauli blocking leads to a plateau of unity filling. The overall shape of the cloud was determined by the trapping potential, which was not perfectly harmonic due to residual large-scale imperfections in our physics lattice beams. Even though the spin-polarized degenerate Fermi gas does not thermalize any more during lattice ramp up, our loading sequence resulted in a state close to a band insulator. Absence of thermalization hinders the redistribution of population from the first excited into the lowest band, which most likely limits the flatness of the observed density plateau. The atoms in the excited band accumulate in the trap center, where we detected an increased number of doubly occupied sites.

The incompressibility of the band insulator manifests itself locally as a suppression of on-site atom number fluctuations $\Delta n_i^2 = \langle \hat{n}_i^2 \rangle - \langle \hat{n}_i \rangle^2$ below the Poissonian variance given by $\langle \hat{n}_i \rangle$, expected for uncorrelated atoms. Indeed, in the region of the density plateau we found strongly suppressed fluctuations with a normalized variance $\Delta n_i^2 / \langle \hat{n}_i \rangle = -11.9^{+1.6}_{-2.7}$ dB [see Fig. 3(b)], while the Poisson limit was recovered in the low density wings.

Enabled by the site resolved measurement of the lattice occupations and under reasonable assumptions on the

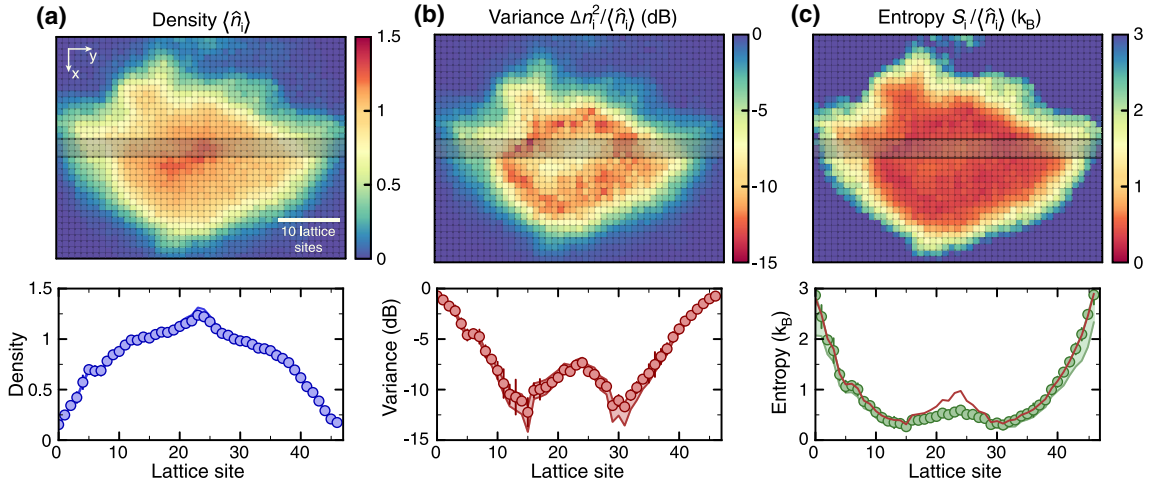

FIG. 3 (color online). Local statistical analysis. We analyze the local, single-site resolved occupation statistics of 425 images. Each pixel corresponds to a physics lattice site in the 2D histograms shown in the top row. Bottom row: horizontal cuts averaged over the vertical three sites indicated by the transparent box above. The shaded regions correspond to the systematic uncertainty in the local population assignment during reconstruction. Statistical error bars represent one standard deviation. (a) Average density. Pauli blocking results in a large region of approximately uniform density around the center. (b) Normalized atom number fluctuations. The band insulator manifests itself in the suppression of fluctuations most strongly in the region of approximately flat density in (a). In the wings of the cloud, Poissonian statistics is recovered. (c) Entropy per atom. The lowest entropies of $0.3k_B$ are found in a ring around the center. The entropy increases towards the center and the edge due to the increase of double occupancies and holes, respectively. The red line is the result for the entropy, when assuming four instead of two accessible single particle states per site.

accessible local quantum states, we reconstructed the local entropy S_i, without relying on a local density approximation or thermal equilibrium. The entropy per site $S_i/k_B = -\sum_E p_E^{(i)} \ln p_E^{(i)}$ was calculated from the occupation probabilities $p_E^{(i)}$ of all many-body energy eigenstates allowed for a given number of identical fermions distributed over k single particle states. Based on our observations, we limited the analysis to maximally two atoms per site. For noninteracting fermions, the probabilities p_E are directly related to the measured probabilities of finding zero, one or two atoms per site [21]. Here, we ignored the finite tunneling, which couples the different single particle states, leading to an overestimation of the inferred entropy. The number of populated single particle states was not directly accessible. Therefore, we analyzed the simplest case $k = 2$, and a second, maximal entropy scenario of $k = 4$, assuming the local ground state and three equally populated excited states, one per spatial direction. In Fig. 3(c), we present the resulting entropy distribution normalized to the mean site occupation. The two cases $k = 2$ and $k = 4$ converge in the limit of low double occupancy, showing that the entropy can be faithfully reconstructed in this regime. We extracted a minimum entropy per atom of $S_i/\langle n_i \rangle = 0.3(1)k_B$ in the density plateau region, while it increased towards the edge and the center, where the probability to find holes or two atoms was enhanced, respectively.

An upper limit to the temperature in the two-dimensional harmonic trap T_{ini} prior to lattice ramp-up can be deduced from the entropy measurement in the lattice. Based on the experimentally determined total entropy $\sum_i S_i = 1.05(5)Nk_B$, we obtained $T_{\mathrm{ini}}/T_F = 0.16(1)$, where T_F is the Fermi temperature [32,33].

Our measurements described before reveal above unity filling in the center of the clouds. Contrary to earlier experiments [12,14,34], this observation indicates a suppression of parity projection, that is, the rapid loss of pairs of atoms in the same lattice site during fluorescence imaging. To set an upper bound on the probability for parity projection, we increased the density of the spin-polarized sample at constant atom number and measured the change in fluorescence and local site occupations. The density was controlled by the confinement in the initial harmonic trap, in which the gas was still in thermal equilibrium at chemical potential μ. When ramping up the optical lattice, the atomic sample cannot thermalize. Consequently, population above the energy E_R, around which the band gap opens, was transferred into the first excited band. Hence, the filling factor in the center of the lattice increased with increasing μ. We indeed observed a compression of the cloud and a strong increase of the fluorescence level in the center of the cloud, but no measurable change in the total fluorescence signal [see Fig. 4(a)]. This provides strong evidence for a small probability of parity projection and that the photon scattering rate is constant, even when adjacent pinning lattice sites were filled—an important prerequisite for the detection of higher site occupations. In Fig. 4(b) we compare the fraction x_2 of doubly occupied to the fraction x_0 of empty sites. For the strongest compression, their values reach $x_2 = 0.3^{+0.1}_{-0.05}$ and $x_0 = 0.020(5)$, resulting in an upper limit to parity projection of 9%.

This observed suppression of parity projection is explained by the loading from the physics into the pinning lattice. Because of the shorter lattice constant of the pinning lattice, the number of states per Brillouin zone is increased compared to the physics lattice. When switching on the much deeper pinning lattice, states in the first excited band of the physics lattice connect to states in the lowest band of the pinning lattice. Hence, initial double occupancies are separated into different pinning lattice sites as long as the switch on of the pinning lattice is adiabatic, which we ensured in our experiments.

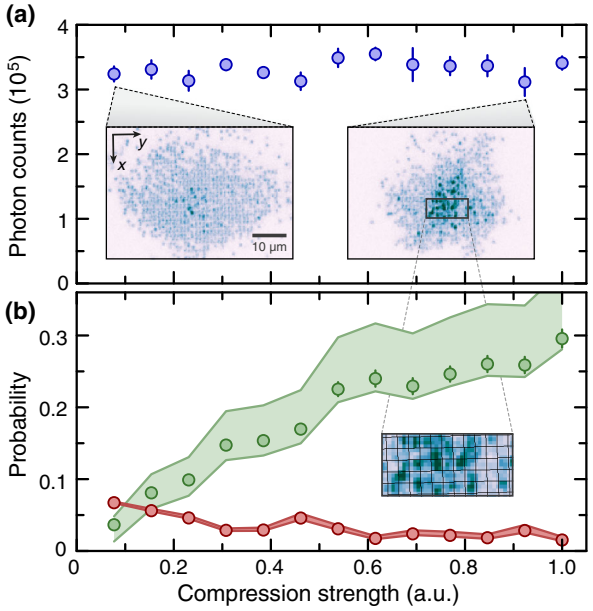

FIG. 4 (color online). Absence of parity projection. (a) Overall fluorescence level. We observe a constant total fluorescence level while increasing the density by trap compression. Insets: Representative images for two different compression strengths. Approximately unity filling is observed for weak compression, whereas for stronger confinement a dense core of multiply occupied sites is visible. (b) Probability of empty (red) and doubly (green) occupied sites versus compression strength. The number of holes decreases despite an increase in the number of doubly occupied sites. The shaded area corresponds to the systematic uncertainty in the local population assignment during reconstruction. Inset: Close-up of the central region marked by the black box in (a), demonstrating the localization of high fluorescence regions to individual lattice sites. Error bars are one standard deviation of the mean.

In conclusion, we presented a site-resolved statistical study of single component degenerate fermionic lattice gases, directly demonstrating Pauli blocking in a textbook-like experiment. Additionally, we introduced a novel quantum gas microscope for fermionic ^{6}Li, which separates the detection system from the physical system under study. Not only does it provide a way to circumvent parity projection, but it is also directly applicable to more advanced lattice geometries, such as superlattices. In the future, we expect it to give access to the local full counting statistics, even spin resolved. Combining such spin-resolved detection with local manipulation of the quantum gas [35] will enable a new generation of experiments with fermionic quantum matter that can range from the study of multipoint correlation functions [36], measurement of exotic quasiparticles and their dynamics [37] to advanced probing of nonequilibrium dynamics in many-body systems.

We thank S. Blatt and M. Greiner for helpful discussions and M. Lohse, T. Gantner, and T. Reimann for technical assistance while building the experimental setup. We acknowledge funding by the MPG and EU (UQUAM).

*ahmed.omran@mpq.mpg.de

[1] A. G. Truscott, K. E. Strecker, W. I. McAlexander, G. B. Partridge, and R. G. Hulet, Science **291**, 2570 (2001).
[2] T. Müller, B. Zimmermann, J. Meineke, J.-P. Brantut, T. Esslinger, and H. Moritz, Phys. Rev. Lett. **105**, 040401 (2010).
[3] C. Sanner, E. J. Su, A. Keshet, R. Gommers, Y.-i. Shin, W. Huang, and W. Ketterle, Phys. Rev. Lett. **105**, 040402 (2010).
[4] W. D. Oliver, J. Kim, R. C. Liu, and Y. Yamamoto, Science **284**, 299 (1999).
[5] M. Henny, S. Oberholzer, C. Strunk, T. Heinzel, K. Ensslin, M. Holland, and C. Schönenberger, Science **284**, 296 (1999).
[6] H. Kiesel, A. Renz, and F. Hasselbach, Nature (London) **418**, 392 (2002).
[7] M. Iannuzzi, A. Orecchini, F. Sacchetti, P. Facchi, and S. Pascazio, Phys. Rev. Lett. **96**, 080402 (2006).
[8] T. Rom, T. Best, D. van Oosten, U. Schneider, S. Fölling, B. Paredes, and I. Bloch, Nature (London) **444**, 733 (2006).
[9] T. Jeltes, J. M. McNamara, W. Hogervorst, W. Vassen, V. Krachmalnicoff, M. Schellekens, A. Perrin, H. Chang, D. Boiron, A. Aspect, and C. I. Westbrook, Nature (London) **445**, 402 (2007).
[10] N. Gemelke, X. Zhang, C.-L. Hung, and C. Chin, Nature (London) **460**, 995 (2009).
[11] W. S. Bakr, A. Peng, M. E. Tai, R. Ma, J. Simon, J. I. Gillen, S. Fölling, L. Pollet, and M. Greiner, Science **329**, 547 (2010).
[12] J. F. Sherson, C. Weitenberg, M. Endres, M. Cheneau, I. Bloch, and S. Kuhr, Nature (London) **467**, 68 (2010).
[13] K. D. Nelson, X. Li, and D. S. Weiss, Nat. Phys. **3**, 556 (2007).
[14] W. S. Bakr, J. I. Gillen, A. Peng, S. Fölling, and M. Greiner, Nature (London) **462**, 74 (2009).
[15] M. F. Parsons, F. Huber, A. Mazurenko, C. S. Chiu, W. Setiawan, K. Wooley-Brown, S. Blatt, and M. Greiner, Phys. Rev. Lett. **114**, 213002 (2015).
[16] E. Haller, J. Hudson, A. Kelly, D. A. Cotta, B. Peaudecerf, G. D. Bruce, and S. Kuhr, Nat. Phys. **11**, 738 (2015).
[17] L. W. Cheuk, M. A. Nichols, M. Okan, T. Gersdorf, V. V. Ramasesh, W. S. Bakr, T. Lompe, and M. W. Zwierlein, Phys. Rev. Lett. **114**, 193001 (2015).
[18] G. J. A. Edge, R. Anderson, D. Jervis, D. C. McKay, R. Day, S. Trotzky, and J. H. Thywissen, arXiv:1510.04744.
[19] P. M. Preiss, R. Ma, M. E. Tai, J. Simon, and M. Greiner, Phys. Rev. A **91**, 041602 (2015).
[20] T. Fukuhara, S. Hild, J. Zeiher, P. Schauß, I. Bloch, M. Endres, and C. Gross, Phys. Rev. Lett. **115**, 035302 (2015).
[21] See Supplemental Material http://link.aps.org/supplemental/10.1103/PhysRevLett.115.263001 for detailed information, which includes Ref. [22].
[22] M. S. Safronova, U. I. Safronova, and C. W. Clark, Phys. Rev. A **86**, 042505 (2012).
[23] P. M. Duarte, R. A. Hart, J. M. Hitchcock, T. A. Corcovilos, T.-L. Yang, A. Reed, and R. G. Hulet, Phys. Rev. A **84**, 061406 (2011).
[24] J. Sebastian, C. Gross, K. Li, H. C. J. Gan, W. Li, and K. Dieckmann, Phys. Rev. A **90**, 033417 (2014).
[25] C. Chin, R. Grimm, P. Julienne, and E. Tiesinga, Rev. Mod. Phys. **82**, 1225 (2010).
[26] M. D. Shotter, Phys. Rev. A **83**, 033617 (2011).
[27] C. Monroe, D. M. Meekhof, B. E. King, S. R. Jefferts, W. M. Itano, D. J. Wineland, and P. Gould, Phys. Rev. Lett. **75**, 4011 (1995).
[28] S. E. Hamann, D. L. Haycock, G. Klose, P. H. Pax, I. H. Deutsch, and P. S. Jessen, Phys. Rev. Lett. **80**, 4149 (1998).
[29] A. J. Kerman, V. Vuletić, C. Chin, and S. Chu, Phys. Rev. Lett. **84**, 439 (2000).
[30] Y. S. Patil, S. Chakram, L. M. Aycock, and M. Vengalattore, Phys. Rev. A **90**, 033422 (2014).
[31] B. J. Lester, A. M. Kaufman, and C. A. Regal, Phys. Rev. A **90**, 011804 (2014).
[32] L. D. Carr, G. V. Shlyapnikov, and Y. Castin, Phys. Rev. Lett. **92**, 150404 (2004).
[33] Y. Castin, in *Ultra-Cold Fermi Gases*, edited by M. Inguscio, W. Ketterle, and C. Salomon (Società Italiana Di Fisica, Bologna, Italy 2007).
[34] M. T. DePue, C. McCormick, S. L. Winoto, S. Oliver, and D. S. Weiss, Phys. Rev. Lett. **82**, 2262 (1999).
[35] C. Weitenberg, M. Endres, J. F. Sherson, M. Cheneau, P. Schauß, T. Fukuhara, I. Bloch, and S. Kuhr, Nature (London) **471**, 319 (2011).
[36] M. Endres, M. Cheneau, T. Fukuhara, C. Weitenberg, P. Schauß, C. Gross, L. Mazza, M. C. Bañuls, L. Pollet, I. Bloch, and S. Kuhr, Science **334**, 200 (2011).
[37] M. Cheneau, P. Barmettler, D. Poletti, M. Endres, P. Schauß, T. Fukuhara, C. Gross, I. Bloch, C. Kollath, and S. Kuhr, Nature (London) **481**, 484 (2012).